Design, synthesis, and photovoltaic performance of regioisomeric D18 – Impact of cross-conjugation on electronic structure and solar cell efficiency

Kaat Valkeneers[a,b,c], Laura Leten[a,b,c], Sam Gielen[a,b,c], Tom Cardeynaels[a,b,c,d], Sigurd Mertens[a,b,c], Jochen Vanderspikken[a,b,c], Ruth Theresia Arwani[e], Adam Marks[e], Alberto Salleo,[e] Rachith Shanivarasanthe Nithyananda Kumar[a,b], Laurence Lutsen[a,b,c], Koen Vandewal[a,b,c,*], Wouter Maes[a,b,c,*]

[a] *Hasselt University, Institute for Materials Research (imo-imomec), Martelarenlaan 42, B-3500 Hasselt, Belgium*

[b] *imec, imo-imomec, Wetenschapspark 1, B-3590 Diepenbeek, Belgium*

[c] *Energyville, imo-imomec, Thorpark 8320, B-3600 Genk, Belgium*

[d] *University of Namur, Laboratory of Theoretical Chemistry, Theoretical and Structural Physical Chemistry Unit, Namur Institute of Structured Matter, Rue de Bruxelles 61, 5000 Namur, Belgium*

[e] *Department of Materials Science and Engineering, Stanford University, Stanford, California 94305, United States*

Abstract

The unrivaled structural tunability of organic semiconductors allows to tailor their chemical and physical properties for distinct optoelectronic applications. This is particularly true for push-pull conjugated polymers, in which the (hetero)aromatic monomers, substituents, and side chains can be readily adapted. On the other hand, the impact of isomerization within the polymer backbone remains poorly explored. Here, a novel structural isomer of the state-of-the-art push-pull copolymer D18 is synthesized. This 'isoD18' regioisomer shows significantly different optical and electrochemical properties. Its deeper highest occupied molecular orbital energy level and reduced non-radiative voltage losses afford a higher open-circuit voltage (from 0.86 to 0.92 V) for the resulting polymer solar cells. Unfortunately, this is accompanied by a decrease in the short-circuit current density and fill factor, which can mainly be attributed to the one-order-lower hole mobility of isoD18, in line with its reduced thin-film organization. Although the performance of the devices based on the isomeric derivative turns out to be lower in this case, this study does enhance our insights into the effects of regioisomerism in polymer semiconductors on the resulting optoelectronic material and device features.

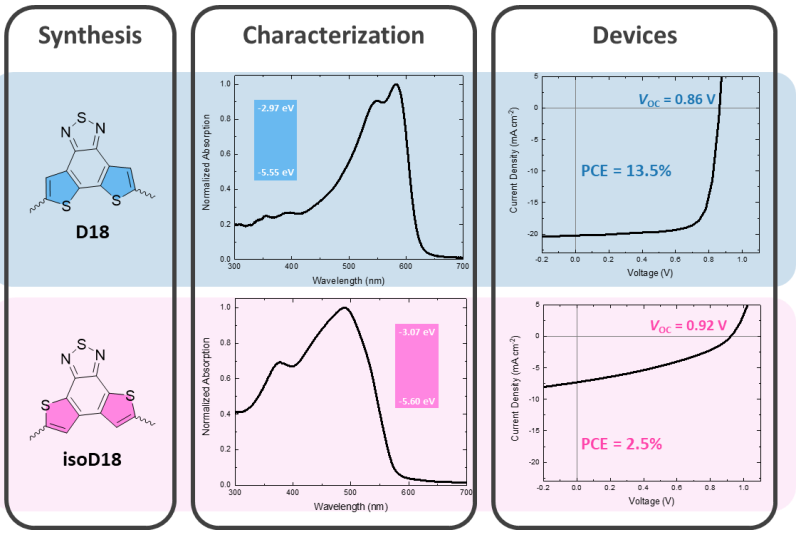

1. Introduction

Over the last three decades, a large number of novel conjugated polymers have been synthesized, in particular for organic photovoltaics (OPV), employing specific structural modifications to optimize their chemical, physical, and optoelectronic properties.[1] These changes predominantly involve alterations in the monomer building blocks and the side chains, sometimes combined with particular substitutions such as halogenation.[2] Another, much less explored option involves the use of structural isomers of the constituent monomers, more specifically regioisomers. A few groups have explored different substitution positions and various linking options between the (hetero)aromatic subunits within the polymer backbone, resulting in changes in the frontier molecular orbital energy levels as well as structural planarity, affecting the π-π stacking behavior.[3] On the other hand, regioisomerism can also entail the fusion pattern of the heterocycles. This strategy has been utilized within specific classes of conjugated polymers, including isomers of benzodithiophene,[4] thienothiophene,[5] and terselenophene,[6] and the resulting materials were tested for various applications, also beyond OPV, such as organic field-effect transistors (OFETs) and theranostics. Müllen *et al.* synthesized five different polymers incorporating various benzodithiophene regioisomers, copolymerized with alkylated bithiophene, and they observed a correlation between the backbone curvature and the semiconducting properties.[4] A large curvature reduced the solid-state order, leading to lower charge carrier mobilities in OFETs, while the less curved structures showed too low solubility for processing, concluding that an intermediate degree of curvature is optimal. In 2015, Chochos *et al.* prepared two conjugated polymers based on isomeric structures of thienothiophene (thieno[3,2-*b*]thiophene and thieno[2,3-*b*]thiophene) and tested these in organic solar cells.[5a] They observed a blue-shift of the absorption spectrum for the thieno[2,3-*b*]thiophene based polymer, correlated to cross-conjugation in the polymer backbone (see **Figure S1**). This cross-conjugation induces a distortion of the quinoidal form, resulting in different optical, electrochemical, structural, and charge transport properties. Despite these significant differences, both isomers gave similar power conversion efficiencies (PCEs) in polymer solar cells. Last year, Li's group reported an isomer of the commonly used 2,1,3-benzothiadiazole, where the positions of the nitrogen and sulfur atoms were swapped.[7] This structural alteration enhanced the extinction coefficient of the resulting donor polymer, the crystallinity of the donor:acceptor blend, and the open-circuit voltage (V_{OC}) of the photovoltaic devices. Consequently, this led to an efficiency increase from 12.9% for the original material to 19% for the regioisomer, one of the highest PCEs for binary OPV devices. These examples illustrate that even a small change in the monomer structure can have a significant impact on the polymer and device properties. However, predicting the outcome of such minor structural alterations remains very challenging and calls for additional examples and studies.

With this in mind, we designed and synthesized a regioisomer of the benchmark OPV donor polymer D18 (termed isoD18; **Figure 1**) and investigated its photovoltaic performance. D18 is a notorious wide bandgap copolymer first reported by Ding *et al.* in 2020.[8] With a maximum solar cell efficiency of 18.2% when combined with the non-fullerene acceptor (NFA) Y6, this polymer was the best performing donor material at that time. Apart from an older patent,[9] the regioisomer of the dithieno[3',2':3,4;2'',3'':5,6]benzo[1,2-*c*][1,2,5]thiadiazole (pull) monomer has, to the best of our knowledge, not been reported yet. We hypothesized that the novel isoD18 polymer would have a blue-shifted absorption and could hence be of interest for indoor OPV,[10] of particular interest for devices connected to the internet of things. Polymer and device analysis indicated that the absorption spectrum indeed shifts hypsochromically and the V_{OC} of the isoD18:Y6 devices increases compared to the D18:Y6 solar cells due to a reduction in non-radiative voltage losses. However, the lower fill factor (FF) and short-circuit current density (J_{SC}) lead to a (strongly) decreased PCE, from 14.3% to 2.7%. This performance difference can be explained by the much lower hole mobility of isoD18, associated to a reduced solid-state ordering, together with the presence of more shunt pathways.

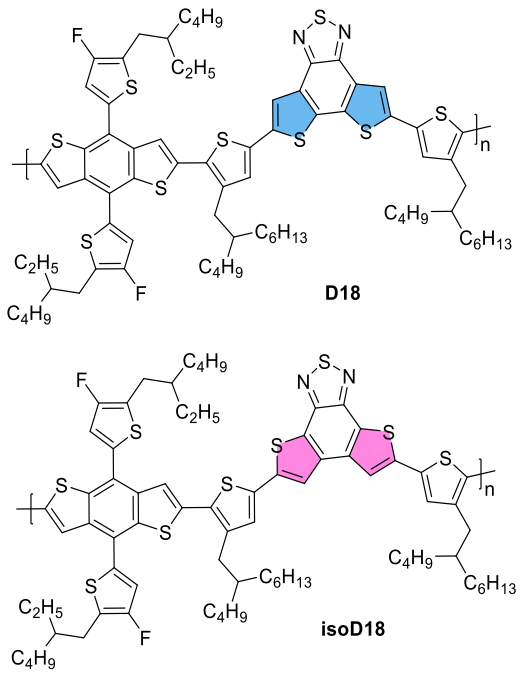

Figure 1 | Chemical structures of the state-of-the-art push-pull copolymer D18 and its regioisomer isoD18, with the colored rings highlighting the different fusion pattern.

2. Results and discussion

The core of the isomeric acceptor monomer of D18 was prepared according to a patent procedure[9] and the synthetic protocol is depicted in **Scheme 1**. The synthesis commenced with a two-fold Friedel-Crafts acylation using oxalyl chloride, resulting in the formation of benzo[1,2-*b*:4,3-*b'*]dithiophene-4,5-dione (**2**). Subsequently, a two-step one-pot reaction was conducted, where hydroxyl amine afforded the dioxime, which was then reduced to diamine **3** employing hydrazine hydrate and palladium on carbon. This (quite unstable) diamine was promptly subjected to a ring closure reaction with thionyl chloride, furnishing dithieno[2',3':3,4;3'',2'':5,6]benzo[1,2-*c*][1,2,5]thiadiazole (**4**) in 30% yield. Precursor **4** was then brominated with molecular bromine to obtain product **5**. The reaction yield was strongly dependent on the purity of the starting material **4** (with the best yield being 68%). Then, coupling of 5,8-dibromodithieno[2',3':3,4;3'',2'':5,6]benzo[1,2-*c*][1,2,5]thiadiazole (**5**) and (4-(2-butyloctyl)thiophen-2-yl)trimethylstannane was accomplished *via* a standard Stille reaction. The poor solubility of compound **5** in organic solvents prevented its complete purification, which likely accounts for the rather low yield (30%) of this Stille cross-coupling. Bromination with *N*-bromosuccinimide (NBS) then resulted in the final monomer, obtained in a yield of 74% after purification *via* preparative (recycling) size exclusion chromatography.

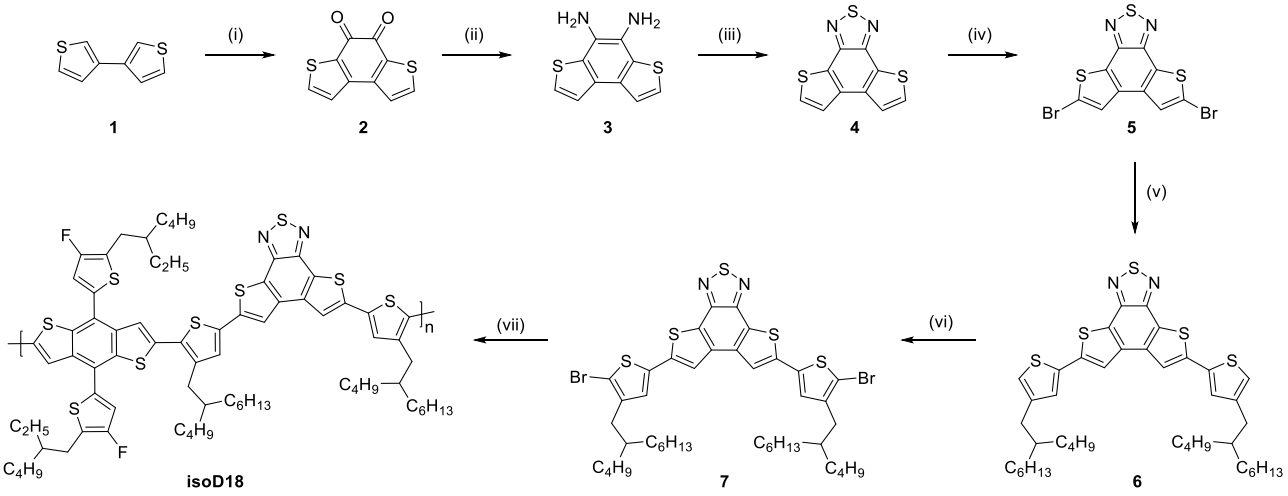

Scheme 1 | Synthesis of isoD18: (i) oxalyl chloride, dichloroethane (88%); (ii) 1. $NH_2OH{\cdot}HCl$, EtOH:pyridine, 2. Pd/C, $N_2H_4{\cdot}H_2O$, EtOH (90%); (iii) $SOCl_2$, Et_3N, $CHCl_3$ (30%); (iv) Br_2, AcOH:$CHCl_3$ (68%); (v) (4-(2-butyloctyl)thiophen-2-yl)trimethylstannane, $Pd(PPh_3)_4$, DMF (30%); (vi) NBS, CH_2Cl_2 (74%); (vii) Pd_2dba_3, P(*o*-tol)$_3$, (4,8-bis(5-(2-ethylhexyl)-4-fluorothiophen-2-yl)benzo[1,2-*b*:4,5-*b'*]dithiophene-2,6-diyl)bis(trimethylstannane), toluene (82%).

The brominated monomer **7** was copolymerized with (4,8-bis(5-(2-ethylhexyl)-4-fluorothiophen-2-yl)benzo[1,2-*b*:4,5-*b'*]dithiophene-2,6-diyl)bis(trimethylstannane) *via* a Stille polymerization in toluene with Pd_2dba_3-P(*o*-tol)$_3$ as the catalytic system, affording the novel push-pull copolymer isoD18 (**Scheme 1**). The polymer was purified *via* successive Soxhlet extractions with methanol, acetone, hexanes, dichloromethane, and chloroform.

Possible structural defects in the polymers were analyzed using matrix-assisted laser desorption/ionization – time-of-flight (MALDI–ToF) mass spectrometry (**Figure S6**). Molar masses up to 7600 kDa could be observed, and mostly hydrogen and methyl 'inactive' end groups were identified, as often seen for Stille polymerizations.[11] No major signals of homocoupled species were identified, similar to D18.[12] The molar mass of the polymer was further analyzed using high-temperature gel permeation chromatography (**Figure S7**), indicating a number-average molar mass (M_n) of 27.6 kDa, and a rather narrow dispersity ($Đ$ = 1.5), as compared to 39.2 kDa and a dispersity of 3.3 for the commercial D18 sample used in this study. The frontier molecular orbital energies of both polymers were estimated *via* cyclic voltammetry (CV) (**Table 1**, **Figure S8**, **S9**). Altering the isomeric core resulted in a lower energy for the lowest unoccupied molecular orbital (LUMO) of isoD18 (-3.07, vs. -2.97 eV for D18), while the energy for the highest occupied molecular orbital (HOMO) was slightly lower as well (-5.60 eV, vs. -5.55 eV for isoD18). The absorption spectra of D18 and isoD18 in chloroform solution and in film are presented in **Figure S9**. A blue-shift of 98 nm for the absorption maximum, translating into an enlarged optical gap of 2.15 eV, and significant peak broadening were observed for isoD18.

Table 1 | Overview of the molar mass, optical, and electrochemical properties of D18 and isoD18.

Polymer	HOMO (eV)[a]	LUMO (eV)[a]	$\Delta E_{g,opt}$ (eV)[b]	$\lambda_{max,film}$ (nm)	M_n (kDa)	$Đ$
D18	-5.55	-2.97	1.98	582	39.2	3.3
isoD18	-5.60	-3.07	2.15	488	27.6	1.5

[a] Estimated from cyclic voltammetry (CV) experiments. [b] Based on the absorption onset in the solid-state UV-Vis absorption spectra.

The experimental HOMO-LUMO energies and the observed blue-shift were cross-checked by density functional theory (DFT) calculations of the polymer conformations and the frontier molecular orbitals using M06[13] as the exchange-correlation (XC) functional and 6-31G(d) as the basis set (**Figure 2** and **Figure S10**).

All calculations were performed in the gas phase using the Gaussian16 package.[14] The alkyl side chains were truncated to methyl groups to reduce the calculation time. Even though the dihedral angle between the modified monomer and the linking thiophene does not differ that much (10° for D18 vs. 13° for isoD18; **Figure 2**), the 'anti' conformation of the fused and free thienyl moieties leads to a curved structure for isoD18, which reduces the effective conjugation length and might hinder π-π stacking.[4] Furthermore, for the 'tetramer' of D18 (i.e. 2 repeating units of each monomer), the electron clouds for both the HOMO and LUMO are delocalized over both monomeric subunits, whereas for isoD18 they are clearly more localized on the respective push and pull monomers. The resonance structures of the copolymers also show a shorter conjugated segment for isoD18 due to cross-conjugation (**Figure S2**), which inhibits full delocalization along the polymer backbone. This cross-conjugation, together with the curved polymer backbone, reduces intramolecular charge transfer between the electron-donating and electron-withdrawing building blocks, and thereby explains the ~100 nm blue-shift of the absorption maximum.

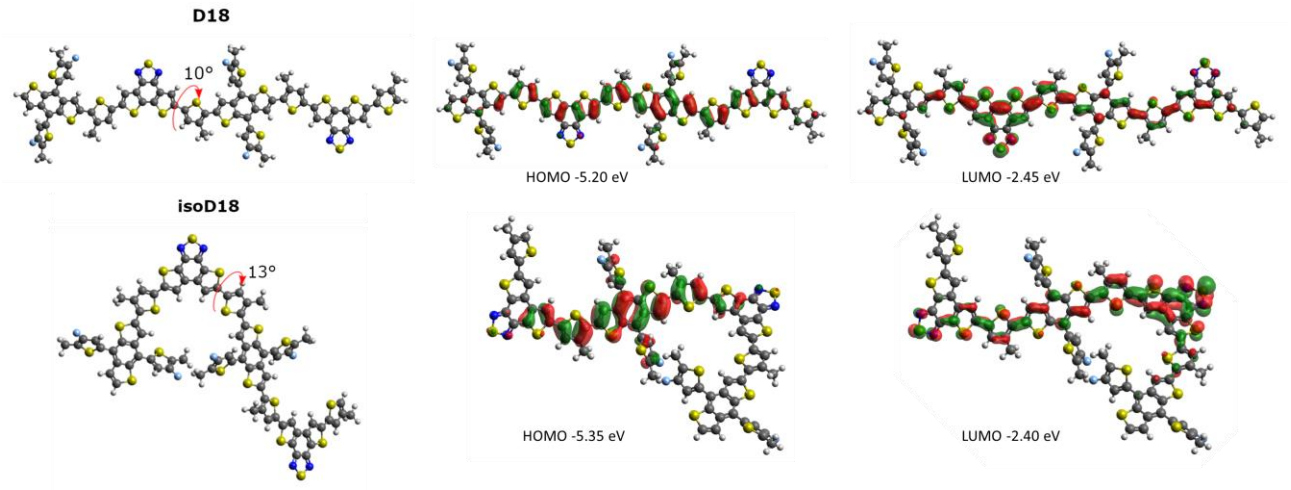

Figure 2 | Conformational analysis (left) and DFT [M06/6-31G(d)] calculated frontier molecular orbitals (HOMO in the middle, LUMO on the right) for 'tetramers' of D18 and isoD18, with the dihedral angles between the modified monomers and the thiophene linkers depicted on the structures.

The photovoltaic properties of isoD18 were then evaluated by incorporating the polymer in a standard device stack (ITO/PEDOT:PSS/active layer/PDINO/Ag) in combination with Y6 as the electron acceptor (ratio 1:1.6). Devices based on D18 were made in parallel to make a fair comparison between the two materials (**Table 2**, **Figure 3a**). The solar cells prepared from isoD18 exhibited an increased V_{OC} of 0.92 V, compared to 0.86 V for D18:Y6. Unfortunately, this improvement in V_{OC} was accompanied by a significant decrease of both the J_{SC} (from 21.96 to 7.91 mA/cm²) and FF (from 0.76 to 0.36), resulting in a strongly decreased PCE, which dropped from 13.48 to 2.49% (on average). The external quantum efficiency (EQE) spectra of the solar cell devices are depicted in **Figure 3b** and show peak values of 60% for the devices based on D18 and only 15% for the solar cells made from isoD18. Several experiments, explained in the following paragraphs, were hence performed to investigate the major cause(s) of this performance difference.

Table 2 | Performance parameters for the OPV devices based on D18 and isoD18.

Active layer	V_{OC} (V)	J_{SC} (mA/cm²)	FF	Av. PCE (%)*	Best PCE (%)
D18:Y6	0.86	21.96	0.76	13.48	14.35
isoD18:Y6	0.92	7.91	0.36	2.49	2.69

* The average PCE values were calculated over 4 devices.

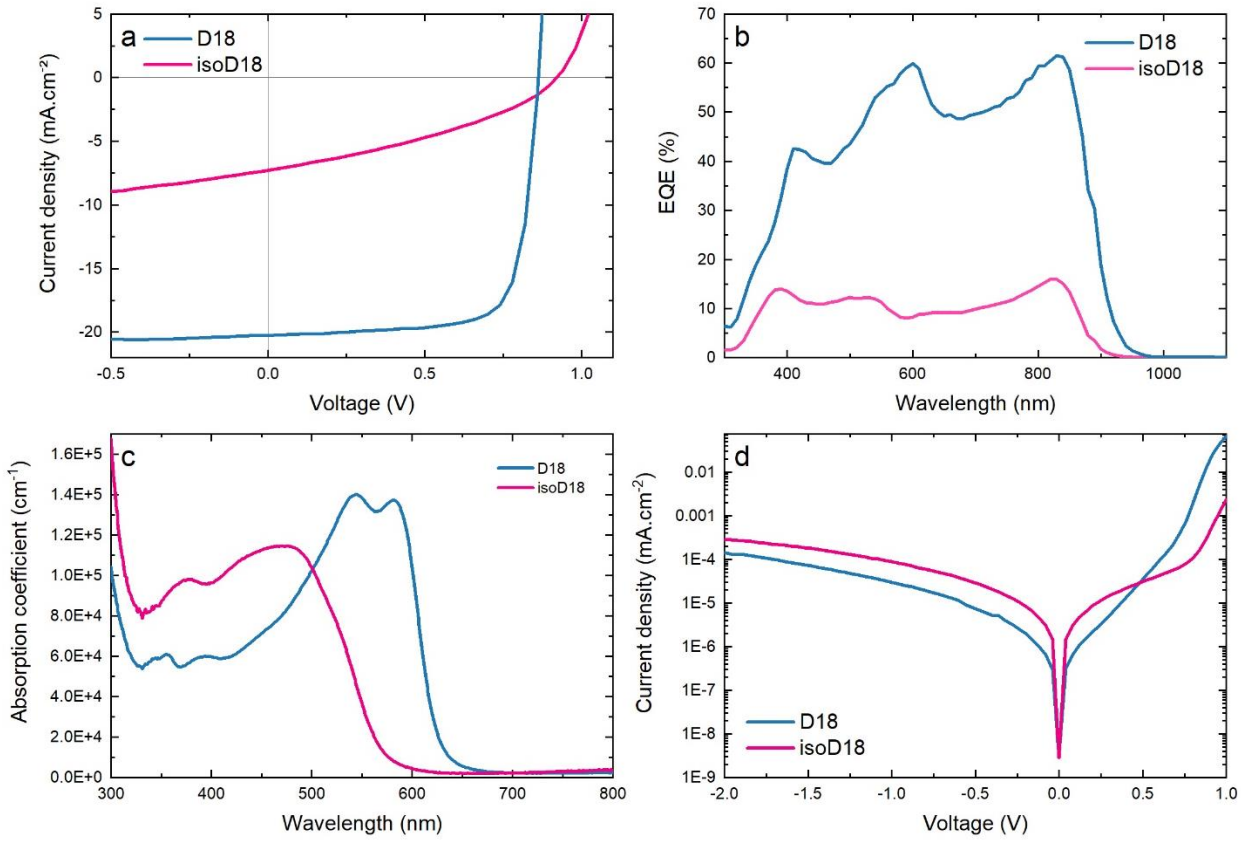

Figure 3 | (a) Current density versus voltage curves under AM1.5 conditions, (b) EQE spectra, (c) absorption coefficients of the neat materials (in film), and (d) current density versus applied voltage curves in the dark for the solar cell devices based on D18:Y6 (blue) and isoD18:Y6 (pink).

First, the V_{OC} enhancement was further analyzed. The non-radiative voltage losses, ΔV_{nr}, of a solar cell represent the reduction in voltage due to the presence of non-radiative recombination. For the ideal solar cell, non-radiative pathways are eliminated, resulting in $\Delta V_{nr} = 0$ and maximizing a cell's V_{OC}. However, for organic devices, ΔV_{nr} values are typically in the order of a few hundred millivolts.[15] Two independent methods were used to accurately determine these losses, as demonstrated before by Benduhn *et al.*[16] The first method measures the quantum yield of the electroluminescent emission (EQE_{EL}), which is directly related to the non-radiative voltage losses via $\Delta V_{nr} = \frac{k_b T}{q} \ln\left(\frac{1}{EQE_{EL}}\right)$. For the second method, a radiative open-circuit voltage (V_{OC}^{Rad}), assuming the absence of the non-radiative recombination, is calculated using a sensitively measured spectrum of the photovoltaic external quantum efficiency (EQE_{PV}). The non-radiative voltage losses are then quantified by the difference between the calculated V_{OC}^{Rad} and the measured V_{OC}. When applied here, both methods result in comparable values: $\Delta V_{nr} = 0.22$ V for the devices based on D18:Y6 and $\Delta V_{nr} = 0.18$ V for isoD18:Y6. Thus, the observed increase in open-circuit voltage by 60 mV for the devices based on isoD18:Y6 can partly be attributed to a reduction in non-radiative voltage losses, with an increase in EQE_{EL} by an order of magnitude, to about 0.1% (**Figure S11c**). This is hence a noticeable positive effect of the regioisomeric structure applied.

To shed light on the significant difference in short-circuit current, we first analyzed the absorption coefficients of the neat polymers in film (**Figure 3c**). Even though the peak absorption coefficient of isoD18 (1.15 x 10^5 cm^{-1}) is slightly lower than the one of D18 (1.40 x 10^5 cm^{-1}), this does not explain the large difference in absolute EQE values for the devices based on both materials. The surface topology of the active layers was analyzed using atomic force microscopy (**Figure S12**). With this technique, domain sizes can be

visualized and the roughness of the active layer can be determined. A rough active layer may indicate a seriously distorted bulk heterojunction morphology, detrimental for the device performance. In this case, no significant difference could be observed for the active layers based on the D18:Y6 and the isoD18:Y6 blends. The samples show an average surface roughness (Ra) of 1.4 and 1.0 nm for the blends based on D18 and isoD18, respectively, and a root-mean-square roughness (Rq) of 1.8 and 1.3 nm.

To verify if limited charge carrier mobility contributes to the poor short-circuit current when applying isoD18, the hole mobilities of both neat polymers were determined using the space-charge-limited current (SCLC) method. As shown in **Figure S13**, the hole mobility of isoD18 (1.88×10^{-4} $cm^2 V^{-1} s^{-1}$) is more than one order of magnitude lower than the one of D18 (3.33×10^{-3} $cm^2 V^{-1} s^{-1}$). This significant difference might be related to the curved backbone of isoD18, as identified by the DFT calculations, and can also explain the drastic lowering of the FF for the devices based on isoD18:Y6.

From literature, it is known that other factors like the series (R_s) and shunt resistance (R_{sh}) have an influence on the FF as well.[17] R_s is mainly described by the resistance of the active layer and electrodes, and the resistance introduced at the interface of these layers. It can be estimated from the inverse derivative of the dark *J-V* curve (**Figure 3d**) near V_{OC} and its value is ideally close to zero. Compared to the 0.06 Ω cm² for the devices based on the D18 variant, the isoD18 cells have an estimated R_s of 1.05 Ω cm². This 18 times higher resistance scales very well with the lower mobility of isoD18. Although there is a significant difference between these two values, only a minor impact on the FF is expected as both series resistances are rather low. The presence of alternate current pathways (pinholes, shorted pathways, traps) that influence the FF can be estimated *via* R_{sh}. This is calculated from the inverse derivative of the dark *J-V* curve near zero volt and ideally approaches infinity. From calculations, it was shown for devices with an R_{sh} above 6×10^3 Ω cm², that the influence on the FF can be neglected.[17] The shunt resistance for the D18:Y6 solar cells was found to be on average 1.6×10^3 Ω cm², compared to 2.7×10^2 Ω cm² for the devices based on isoD18:Y6. The lower shunt resistance (more than one order of magnitude difference compared to the benchmark value of 6×10^3 Ω cm²) for the isoD18-based devices results in a significant decrease in FF. Although the R_{sh} of the D18 device is still below 6×10^3 Ω cm², it is much closer and therefore the impact on the FF will be minimal. This can also be seen in **Figure 3a**, where the slope of the isoD18 *J-V* curve under illumination around 0 V is 2.6×10^2 Ω cm². This similar shunt in the dark and under illumination points to shorted pathways or traps as the reason for a reduced FF. From the above, it can be concluded that the overall performance loss (reduced EQE and FF) for the isoD18-based device stems from the lower hole mobility combined with the presence of more shunt pathways.

To further understand the drastic difference in hole mobility, grazing incidence wide-angle X-ray scattering (GIWAXS) analysis was carried out on both the neat polymers and their blends with Y6 (**Figure 4**; lineouts in **Figure S14**). Neat D18 shows a mixed face- and edge-on orientation relative to the substrate, with a lamellar peak at approximately 0.31 $Å^{-1}$ (20.3 Å) in both the out-of-plane (Q_z) and in-plane (Q_{xy}) directions (**Figure 4a** and **Table S1**). The π-π stacking peak at 1.70 $Å^{-1}$ (3.7 Å) appears most prominently in Q_z, as previously observed in literature.[18] Additionally, a clear (002) backbone peak appears in Q_{xy} at 0.55 $Å^{-1}$ (11.4 Å), indicating good ordering of the polymer chains along the backbone. Furthermore, as observed in literature,[18] another signal appears at 1.08 $Å^{-1}$ due to a higher order scattering of the backbone peak. Neat isoD18 scatters much more isotropically, without any sharp features (**Figure 4b**). A broad (100) lamellar peak is seen at approximately 0.42 $Å^{-1}$ (15.0 Å) in the Q_z direction. Additionally, a very broad signal, most prominently appearing in Q_z at 1.24 $Å^{-1}$ (5.7 Å) may be a result of the less compact π-π stacking of the material. Both the lamellar and π-π stacking signals also show up at similar values in Q_{xy}, displaying the isotropic nature of isoD18. This scattering behavior may be caused by the strong curvature of isoD18 chains, thus hindering the π-π stacking and causing less ordering along the polymer backbone when compared to the D18 polymer. This

hypothesis is further supported by the conformational DFT analysis performed. Consequently, inter- and intra-chain charge transport is expected to be less efficient, resulting in the observed low hole mobility.

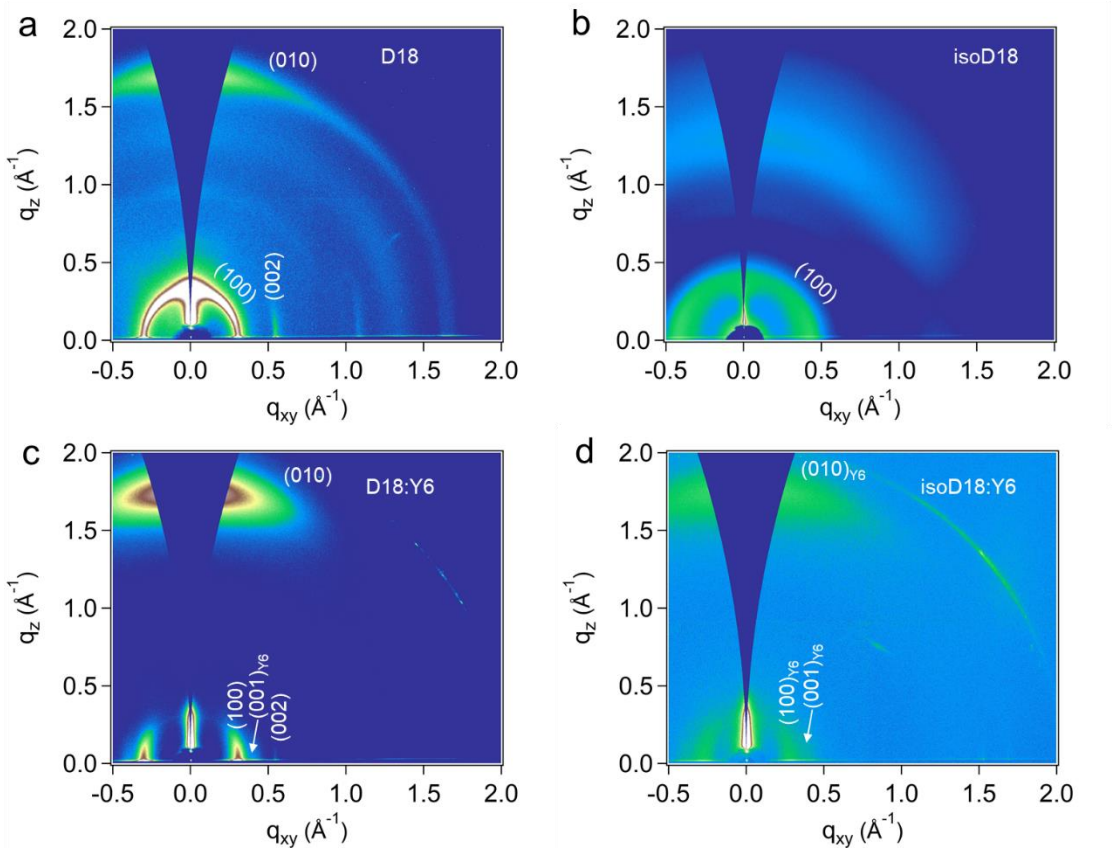

Figure 4 | 2D-GIWAXS spectra for (a) D18, (b) isoD18, (c) D18:Y6, and (d) isoD18:Y6.

For the D18:Y6 blend, a lamellar (100) signal at 0.31 $Å^{-1}$ (20.3 Å) in Q_{xy} is again seen, which may originate from the D18 chains (**Figure 4c**). Moreover, a small shoulder for Y6 at 0.42 $Å^{-1}$ (15.7 Å) can be observed in Q_{xy}, which corresponds to end-group stacking columns as previously determined through single crystal measurements.[19,20] Also, in Q_{xy}, the distinct backbone (002) stacking peak of D18 remains present, indicating good chain ordering along the backbone in the blend. The clear π-π stacking signal in Q_z appearing at 1.74 $Å^{-1}$ (3.6 Å) originates from both D18 and Y6 face-on crystallites and stipulates the dominant face-on orientation of the materials.[18] Similar to the neat polymer, the isoD18:Y6 blend scatters much weaker, resulting in a lower intensity spectrum at comparable sample thickness and indicating a much more amorphous blend (**Figure 4d**; lineouts in **Figure S15**). The observed (coherent) scattering is predominantly from Y6. The face-on orientation of the Y6 crystallites results in a (100) lamellar signal at 0.28 $Å^{-1}$ (22.4 Å), along with the small shoulder of Y6 at 0.42 $Å^{-1}$ in Q_{xy}.[20] Finally, in Q_z, the (010) signal at 1.76 $Å^{-1}$ (3.6 Å) can be attributed to π-π stacking of Y6. The predominant (but weak) appearance of Y6 signals stipulates the general amorphous nature of the blend. This absence of orientation likely hampers inter- and intrachain coupling, thus hindering the formation of efficient charge transport pathways and charge extraction.

Based on the information above, we can now revisit the large difference in EQE observed between the solar cells prepared from D18 and isoD18. **Figure 3** shows that, even though the peak absorption coefficients of isoD18 and D18 are comparable in magnitude and the devices are within the same thickness range, the EQE of the isoD18 device is much lower than that of the D18 device. This is partly because of poor transport and partly because of insufficient exciton dissociation. This could be due to a poor mixing between Y6 and isoD18, which is unlikely given the more disordered nature of isoD18. We therefore postulate that, given the increase

in V_{OC} for the isoD18:Y6 system, Y6 excitons might not experience sufficient driving force to dissociate into free charge carriers due to a decrease in the HOMO energy level of isoD18.

3. Conclusions

A novel regioisomer – isoD18 – of the popular donor polymer D18 was successfully synthesized. Even though the electrochemical bandgap did not change that much, the cross-conjugation pattern and larger backbone curvature of isoD18 resulted in a ~100 nm blue-shift of the absorption maximum in film. When tested in OPV devices, combined with Y6 as the electron acceptor, the isoD18-based solar cells showed a higher V_{OC} of 0.92 V (compared to 0.86 V for the D18-based devices), attributed to minimized non-radiative voltage losses. Unfortunately, this higher V_{OC} was accompanied by a seriously decreased FF and J_{SC}, and therefore a decreased performance, from 13.5% (on average) for D18 to 2.5% for the isoD18-based devices. The origin of this performance drop is a combination of several factors, including a lower hole mobility for isoD18 (1.88×10^{-4} $cm^{-2} V^{-1} s^{-1}$, compared to 3.33×10^{-3} $cm^{-2} V^{-1} s^{-1}$ for D18), in line with its isotropic molecular organization in thin films, and a lower shunt resistance for the isoD18:Y6 blend (2.7×10^{2} Ω cm^2, compared to 1.6×10^{3} Ω cm^2 for D18:Y6). These findings emphasize the significant impact that even small structural changes, such as regioisomerism, can have on the properties of conjugated polymers and the resulting devices. While isoD18 does not come close to D18 in terms of solar cell efficiency, the insights gained from this study offer valuable guidance for future design strategies, particularly in tailoring the optoelectronic properties.

Acknowledgements

The authors thank Huguette Penxten for the CV analysis and Prof. Anitha Ethirajan for access to the AFM equipment. They also thank the Research Foundation – Flanders (FWO Vlaanderen) for continuing financial support (PhD scholarship 1S98320N (Ka.V.), postdoctoral scholarships 1284623N (T.C.) and 1266923N (S.G.), MALDI–ToF infrastructure project I006320N, and the Scientific Research Network 'Supramolecular Chemistry and Materials' W000620N), as well as the European Research Council (grant agreement 864625). Use of the Stanford Synchrotron Radiation Light source, SLAC National Accelerator Laboratory, is supported by the U.S. Department of Energy, Office of Science, Office of Basic Energy Sciences under Contract No. DE-AC02-76SF00515.

Author contributions

Kaat Valkeneers: investigation (materials synthesis and characterization, photovoltaic device fabrication), funding acquisition, visualization, writing – original draft, writing – review & editing. Laura Leten: investigation (materials synthesis and characterization), writing – review & editing. Sam Gielen: investigation (shunt resistance), writing – review & editing. Tom Cardeynaels: investigation (theoretical calculations), writing – review & editing. Sigurd Mertens: investigation (voltage losses), writing – review & editing. Jochen Vanderspikken: investigation (GIWAXS data analysis), writing – review & editing. Ruth Theresia Arwani: investigation (GIWAXS data acquisition), writing – review & editing. Adam Marks: investigation (GIWAXS data acquisition), writing – review & editing. Alberto Salleo: supervision, funding acquisition, writing – review & editing. Rachith Shanivarasanthe Nithyananda Kumar: investigation (AFM), writing – review & editing. Laurence Lutsen: supervision, funding acquisition, writing – review & editing. Koen Vandewal: supervision (device part), funding acquisition, writing – review & editing. Wouter Maes: conceptualization, project administration, supervision (polymer synthesis and characterization), funding acquisition, writing – review & editing.

References

[1] a) C. Liu, L. Shao, S. Chen, Z. Hu, H. Cai, F. Huang, *Progress in Polymer Science* **2023**, *143*, 101711; b) C. An, J. Hou, *Accounts of Materials Research* **2022**, *3,* 540; c) C. An, Z. Zheng, J. Hou, *Chemical Communications* **2020**, *56*, 4750; d) Z. Qiu, B. A. G. Hammer, K. Müllen, *Progress in Polymer Science* **2020**, *100*, 101179.

[2] a) G. Li, M. Al-Hashimi, A. Facchetti, T. J. Marks, *Nature Reviews Materials* **2025**, DOI: 10.1038/s41578-025-00804-3; b) X. Gao, X. Tong, M. Xu, L. Zhang, Y. Wang, Z. Liu, L. Yang, J. Gao, M. Shao, Z. Liu, *Small* **2023**, *19*, 2208217; c) P. Verstappen, J. Kesters, W. Vanormelingen, G. Heintges, J. Drijkoningen, T. Vangerven, L. Marin, S. Koudjina, B. Champagne, J. Manca, L. Lutsen, D. Vanderzande, W. Maes, *Journals of Materials Chemistry A* **2015**, *3*, 2960.

[3] a) C. Mahmoudi, I. Bulut, J. Jing, S. Fall, B. Heinrich, S. Méry, T. Heiser, P. Lévêque, E. Steveler, M. Majdoub, N. Leclerc, *European Journal of Organic Chemistry* **2021**, *22*, 3170; b) B. Fan, M. Li, D. Zhang, W. Zhong, L. Ying, Z. Zeng, K. An, Z. Huang, L. Shi, G. C. Bazan, F. Huang, Y. Cao, *ACS Energy Letters* **2020**, *5*, 2087; d) M. Zhang, X. Zhang, P. Guo, J. Lv, X. Wang, J. Tong, Y. Xia, *Journal of Materials Research* **2019**, *34*, 2057; c) S. Sengupta, U. K. Pandey, E. U. Athresh, *RSC Advances* **2016**, *6*, 73645; e) X. Guo, S. R. Puniredd, B. He, T. Marszalek, M. Baumgarten, W. Pisula, K. Müllen, *Chemistry of Materials* **2014**, *26*, 3595; f) K. Tsurui, M. Murai, S. Y. Ku, C. J. Hawker, M. J. Robb, *Advanced Functional Materials* **2014**, *24*, 7338.

[4] R. Rieger, D. Beckmann, A. Mavrinskiy, M. Kastler, K. Müllen, *Chemistry of Materials* **2010**, *22*, 5314.

[5] a) R. Singh, G. Pagona, V. G. Gregoriou, N. Tagmatarchis, D. Toliopoulos, Y. Han, Z. Fei, A. Katsouras, A. Avgeropoulos, T. D. Anthopoulos, M. Heeney, P. E. Keivanidis, C. L. Chochos, *Polymer Chemistry* **2015**, *6*, 3098; b) I. McCulloch, M. Heeney, M. L. Chabinyc, D. DeLongchamp, R. J. Kline, M. Cölle, W. Duffy, D. Fischer, D. Gundlach, B. Hamadani, R. Hamilton, L. Richter, A. Salleo, M. Shkunov, D. Sparrowe, S. Tierney, W. Zhang, *Advanced Materials* **2009**, *21*, 1091.

[6] Y. Gao, Q. Li, C. Li, L. Gao, H. Chen, T. Liu, Y. Huang, Z. Liu, S. Li, *ACS Applied Materials & Interfaces* **2020**, *12*, 55605.

[7] T. Lin, Y. Hai, Y. Luo, L. Feng, T. Jia, J. Wu, R. Ma, T. A. Dela Pena, Y. Li, Z. Xing, M. Li, M. Wang, B. Xiao, K. S. Wong, S. Liu, G. Li, *Advanced Materials* **2024**, 2312311.

[8] Q. Liu, Y. Jiang, K. Jin, J. Qin, J. Xu, W. Li, J. Xiong, J. Liu, Z. Xiao, K. Sun, S. Yang, X. Zhang, L. Ding, *Science Bulletin* **2020**, *65*, 272.

[9] Z. Liu, S. Hu, B. Liu (Wuhan Institute of Technology, China) *China Patent CN103483559*, **2014**.

[10] L. Xie, W. Song, J. Ge, B. Tang, X. Zhang, T. Wu, Z. Ge, *Nano Energy* **2021**, *82*, 105770.

[11] G. Pirotte, P. Verstappen, D. Vanderzande, W. Maes, *Advanced Electronic Materials* **2018**, *4,* 1700481.

[12] S. Smeets, Q. Liu, J. Vanderspikken, T. J. Quill, S. Gielen, L. Lutsen, K. Vandewal, W. Maes, *Chemistry of Materials* **2023**, *35*, 8158.

[13] Y. Zhao, D. G. Truhlar, *Theoretical Chemistry Accounts* **2007**, *120*, 215.

[14] Gaussian 16, Revision A.03, M. J. Frisch, G. W. Trucks, H. B. Schlegel, G. E. Scuseria, M. A. Robb, J. R. Cheeseman, G. Scalmani, V. Barone, G. A. Petersson, H. Nakatsuji, X. Li, M. Caricato, A. V. Marenich, J. Bloino, B. G. Janesko, R. Gomperts, B. Mennucci, H. P. Hratchian, J. V. Ortiz, A. F. Izmaylov, J. L. Sonnenberg, D. Williams-Young, F. Ding, F. Lipparini, F. Egidi, J. Goings, B. Peng, A. Petrone, T. Henderson, D. Ranasinghe, V. G. Zakrzewski, J. Gao, N. Rega, G. Zheng, W. Liang, M. Hada, M. Ehara, K. Toyota, R. Fukuda, J. Hasegawa, M. Ishida, T. Nakajima, Y. Honda, O. Kitao, H. Nakai, T. Vreven, K. Throssell, J. A. Montgomery, Jr., J. E. Peralta, F. Ogliaro, M. J. Bearpark, J. J. Heyd, E. N. Brothers, K. N. Kudin, V. N. Staroverov, T. A. Keith, R. Kobayashi, J. Normand, K. Raghavachari, A. P. Rendell, J. C. Burant, S. S. Iyengar, J. Tomasi, M. Cossi, J. M. Millam, M. Klene, C. Adamo, R. Cammi, J. W. Ochterski, R. L. Martin, K. Morokuma, O. Farkas, J. B. Foresman, and D. J. Fox, Gaussian, Inc., Wallingford CT, **2016**.

[15] a) Y. Fu, T. H. Lee, Y. C. Chin, R. A. Pacalaj, C. Labanti, S. Y. Park, Y. Dong, H. W. Cho, J. Y. Kim, D. Minami, J. R. Durrant, J. S. Kim, *Nature Communications* **2023**, *14*, 1870; b) M. A. Green, *Progress in Photovoltaics: Research and Applications* **2011**, *20*, 472.

[16] J. Benduhn, K. Tvingstedt, F. Piersimoni, S. Ullbrich, Y. Fan, M. Tropiano, K. A. McGarry, O. Zeika, M. K. Riede, C. J. Douglas, S. Barlow, S. R. Marder, D. Neher, D. Spoltore, K. Vandewal, *Nature Energy* **2017**, *2*, 17053.
[17] B. Qi, J. Wang, *Physical Chemistry Chemical Physics* **2013**, *15*, 8972.
[18] Z. Wang, Z. Peng, Z. Xiao, D. Seyitliyev, K. Gundogdu, L. Ding, H. Ade, *Advanced Materials* **2020**, *32*, 2005386.
[19] G. Zhang, X.-K. Chen, J. Xiao, P. C. Y. Chow, M. Ren, G. Kupgan, X. Jiao, C. C. S. Chan, X. Du, R. Xia, Z. Chen, J. Yuan, Y. Zhang, S. Zhang, Y. Liu, Y. Zou, H. Yan, K. S. Wong, V. Coropceanu, N. Li, C. J. Brabec, J.-L. Bredas, H.-L. Yip, Y. Cao, *Nature Communications* **2020**, *11*, 3943.
[20] K. An, W. Zhong, F. Peng, W. Deng, Y. Shang, H. Quan, H. Qiu, C. Wang, F. Liu, H. Wu, N. Li, F. Huang, L. Ying, *Nature Communications* **2023**, *14*, 2688.